DESIGN OF A HIGH-EFFICIENCY HIGH-RESOLUTION

X-RAY SPECTROMETER

FOR

1s LAMB SHIFT MEASUREMENTS

by

JEFFERSON L. SHINPAUGH

B.S., Kansas State University, 1982

A MASTER'S THESIS

submitted in partial fulfillment of the

requirements for the degree

MASTER OF SCIENCE

Department of Physics

KANSAS STATE UNIVERSITY

1985

Approved by:

Patrick Richard

Major Professor

TABLE OF CONTENTS

LIST OF FIGURES

ACKNOWLEDGEMENTS

I wish to express my deepest gratitude to Professor Parick Richard for his insight and patient guidance that have made this work possible.

I would like to thank Dr. Martin Stockli and Justin Sanders for their valuable contributions to the production for this work.

I would also like to thank Dr. J.M. Hall, Dr. R.T. Dillingham, and Dr. S.L. Varghese for their assistance in the lab and C. Schmeissner, G. Euliss, and W. Waggoner for their friendship and support.

I also thank Janie Torrey, Kim Tracy, and Dea Richard for the typing and preparation of this thesis and I appreciate the assistance of the staff of the James R. MacDonald Laboratory.

Most of all, I wish to thank my family for the immeasurable love and support they have given me throughout graduate school, as well as throughout all endeavors in my life. All my accomplishments are a result of what they have given me.

Chapter I

INTRODUCTION

A. Lamb Shift Measurements

In the mid 1930's experimental evidence arose in optical spectro-scopy studies[1,2] of hydrogen suggesting that the $2s_{1/2}$ and $2p_{1/2}$ electron energy levels do not coincide.[3] However, due to the limited resolution from doppler broadening of the spectral lines, exact inter-pretations of the results could not be made. It was not until 1947 that Lamb and Retherford showed[4] using microwave techniques that the $2s_{1/2}$ and $2p_{1/2}$ levels of hydrogen are actually nondegenerate. This splitting, historically referred to as the Lamb shift, was the first observed deviation from the Dirac theory. According to the Dirac theory the energy levels of one-electron ions can be calculated exactly and will depend only on the principal quantum number n and the total angular momentum quantum number j,[5] thus the degeneracy of the $2s_{1/2}$ and $2p_{1/2}$ levels.

The first explanation of the $2s_{1/2} - 2p_{1/2}$ splitting was given by Bethe[6] as due to the interaction of the electron with the quantized electromagnetic field. Bethe's quantization of the radiation field was one of the initial formalisms in the development of the theory of quantum electrodynamics (QED). QED predicts radiative corrections to the Dirac energy which along with small corrections for nuclear size determine the shift of an energy level, termed the Lamb shift. The effect of these corrections raises s states relative to the other angular momentum states. Figure 1 shows the relative positions of the energy levels of a one-electron ion as given by the Bohr model, the Dirac theory, and the Dirac theory corrected for the Lamb shift.

1

Figure 1. Energy levels for the ground state and first excited state of a one-electron ion as given by the Bohr model, the Dirac theory, and the Dirac theory corrected for the Lamb shift. The energy levels have been scaled for hydrogenlike chlorine for which the Lamb shift has been calculated[7] to be 0.94 and 0.13 eV for the $1s_{1/2}$ and $2s_{1/2}$ states, respectively. The calculated energies of the $Ly\alpha_1$ and $Ly\alpha_2$ transitions are 2962.38 and 2958.55 eV, respectively.

$n=2$ $2p_{3/2}$ $2p_{3/2}$

$2s_{1/2}$

$2s_{1/2}, 2p_{1/2}$ $2p_{1/2}$

$E_D(Ly\alpha_2)$ $E(Ly\alpha_2)$

$E_D(Ly\alpha_1)$ $E(Ly\alpha_1)$

$n=1$

$S(1s)$

$1s_{1/2}$ $1s_{1/2}$

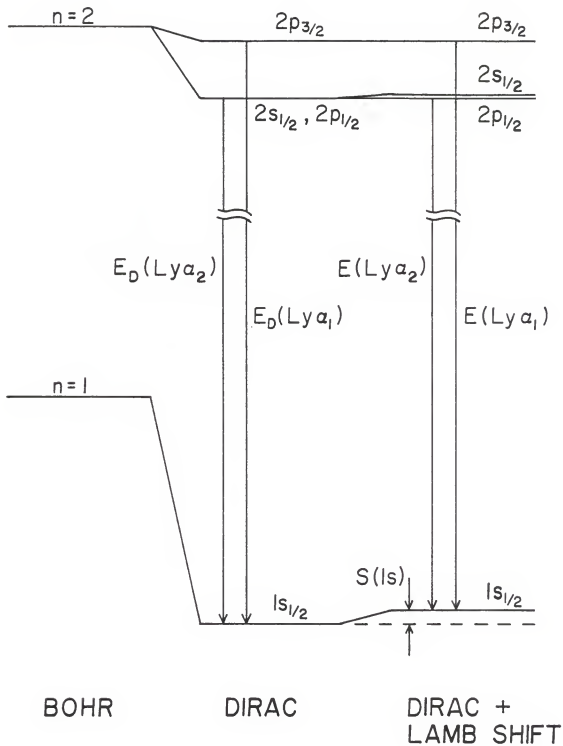BOHR   DIRAC   DIRAC + LAMB SHIFT

3

Figure 1 has been scaled for hydrogenlike chlorine (Z=17) for which the Lamb shift has been calculated[7] to be 0.94 eV for the $1s_{1/2}$ state and 0.13 eV for the $2s_{1/2}$ state.

Measurements of the Lamb shift provide tests of QED predictions and methods of calculation. Most of the measurements have been of the $2s_{1/2} - 2p_{1/2}$ splitting in one-electron ions, since the Lamb shift accounts for the entire separation of these levels. The $2s_{1/2} - 2p_{1/2}$ Lamb shift has been measured in hydrogen to an accuracy within 10 parts per million.[8] Because QED corrections increase with nuclear charge (as approximately Z^4), measurements of the $2s_{1/2} - 2p_{1/2}$ Lamb shift have been extended in Z up to Z=18 for hydrogenlike argon.[9] Even though the heavy-ion measurements are about three orders of magnitude less accurate than hydrogen measurements, it is high-Z Lamb shift measurements that allow for testing of higher order corrections and QED predictions in the domain of high electric fields.

The methods used to measure the $2s_{1/2} - 2p_{1/2}$ Lamb shift, such as electric-field quenching[9] and resonant laser excitation[10] which use the property of the $2s_{1/2}$ state being metastable, are limited in Z. The difficulties of these methods increase with Z due to the decrease of the $2s_{1/2}$ lifetime and ultimately limit the $2s_{1/2} - 2p_{1/2}$ Lamb shift measurements to $Z \leq 20$.[11]

The Lamb shift of the $1s_{1/2}$ level is about eight times larger than that of the $2s_{1/2}$ level due to the approximate n^{-3} scaling. The 1s Lamb shift was first measured in hydrogen in 1975 by Hansch et al.[12] using high-resolution laser spectroscopy. 1s Lamb shift measurements were extended to hydrogenlike heavy ions in 1982 by Briand et al.[13] in hydrogenlike iron (Z=26) and since then have been made up to Z=36 in

hydrogenlike krypton.[14] Experimental determination of the 1s Lamb shift in heavy ions requires the precision measurement of the absolute energies of the Lyman–α x rays ($2p_{1/2,3/2} \rightarrow 1s_{1/2}$ transitions) of one-electron ions. The 1s Lamb shift S(1s), which is a small part ($\leq 0.1\%$) of the total Lyman–α transition energy, can be determined from the difference of the actual (measured) Lyman–α_2 x-ray energy E(Lyα_2) and the calculated Dirac energy E_D(Lyα_2) (corrected for reduced mass) by

$$S(1s) - S(2p_{1/2}) = E_D(Ly\alpha_2) - E(Ly\alpha_2),$$

with a small correction for the $2p_{1/2}$ Lamb shift $S(2p_{1/2})$. A similiar expression gives the 1s Lamb shift from the Lyman–α_1 energy.

The main problems involved in the high-Z Lyman–α energy measurements are inherent to the methods of one-electron ion production. These methods[15] have consisted of foil stripping of high-velocity beams,[16] ionization of gas target atoms (recoil ions) by a highly-charged, high-velocity beam,[17] excitation in a tokamac plasma,[18] and recently, electron-capture from a gas by low-velocity bare ions produced by accel-decel techniques (deceleration of high-velocity bare ions).[19] Although the most accurate measurement (1.5% relative accuracy) of the 1s Lamb shift has been reported by Beyer et al.[17] using argon recoil ions, this method yields high satellite intensities in the Lyman–α spectra due to spectator electrons in the upper levels of the recoil ions. These unresolved satellites introduce difficulties in modeling the spectra to determine the x-ray energies. The method of beam-foil excitation reduces satellite intensities but introduces a large doppler shift in the x-ray energies due to the high

5

velocities needed to produce high-Z one-electron ions. Corrections for the doppler shift require careful spectrometer alignment and accurately known ion velocities. Further comments on the beam-foil method are given in the final chapter of this thesis. Accel-decel techniques should allow for reduced satellite intensities while necessarily reducing doppler effects. The results of this method were being awaited at the time of this writing.

The measurements of the Lyman-α energies for 1s Lamb shift determinations have been made using high-resolution crystal spectrometers. This thesis describes the design and testing of one such spectrometer to be used for 1s Lamb shift measurements in hydrogenlike chlorine. The motivation for building this spectrometer stems from previous work done by Richard et al.[16] using a similar spectrometer for this mesurement. The new spectrometer allows for better resolution which should result in a more accurate measurement of the 1s Lamb shift.

B. High-Resolution X-ray Spectroscopy

When high intensities of x rays are available, very accurate wavelength measurements can be made with high-precision double-crystal spectrometers. These are low-efficiency devices due to the high intensity loss from despersing the x rays through two crystals. In many spectroscopy studies, low intensities dictate the use of less precise, more efficient single-crystal spectrometers. Such is the case in measurements of high-Z Lyman-α energies, since the one-electron ions are produced in low quantities.

One technique that has been widely used in high-resolution x-ray spectroscopy has involved scanning spectrometers. In this type of spectrometer, the crystal is rotated at an angle θ relative to the

incident x rays while the detector is rotated about the crystal at an angle 2θ. The detector, which has a small acceptance window, receives x rays that are diffracted from the crystal as the Bragg angle θ is varied in small, precisely controlled increments. In this manner the spectrum is acquired one interval at a time.

Efficiency in crystal spectrometers can be increased with the use of curved crystals. This type of crystal possesses a focal circle, called the Rowland circle, defined by the bent crystal planes that allows for x rays originating from a source point on the Rowland circle to be focused at an image point that is symmetric to the source point with respect to the crystal and the center of the Rowland circle. X rays of a given wavelength satisfying the Bragg condition are reflected over the entire crystal face and focused at the image point, increasing the intensity of the reflected x rays over that obtained by a flat crystal. Figure 2 shows the path of x rays of two different energies E_1 and E_2 ($E_1 > E_2$) emitted from source points S_1 and S_2, respectively, reflected from a curved crystal and focused on the Rowland circle at I_1 and I_2. For a scanning curved-crystal spectrometer, the source is located at a fixed position while the crystal and the detector are stepped along the Rowland circle to acquire the spectrum. The problems involved in the scanning technique arise from intensity fluctuations in the source and from high background counts during the typically long period of the scan.

The spectrometer that has been built for the chlorine 1s Lamb shift measurements utilizes a curved crystal and a position sensitive x-ray detector. In this method an extended source located inside of the Rowland circle emits x rays that are reflected from the crystal

Figure 2. Path of x rays (shaded area) of energies E_1 and E_2 ($E_1 > E_2$) emitted from source points S_1 and S_2, respectively, reflected from a curved crystal and focused on the Rowland circle at I_1 and I_2.

CURVED CRYSTAL

I_1

I_2

S_1

S_2
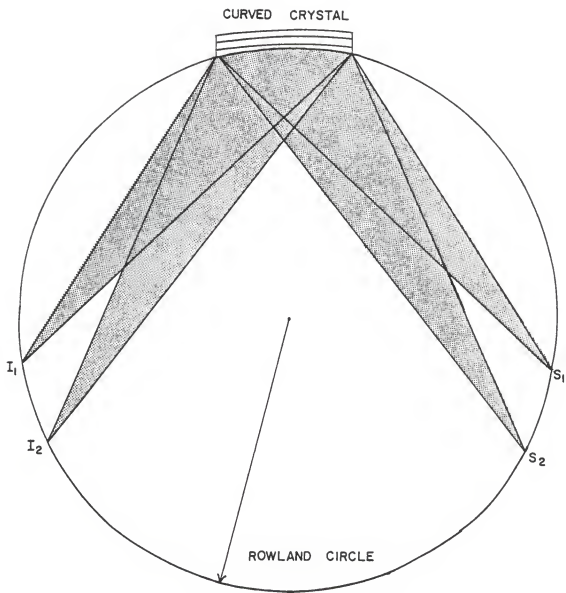
ROWLAND CIRCLE

and focused at the position sensitive detector lying on the Rowland circle (Figure 3). The intensity of a given energy is reduced by placing the source inside of the Rowland circle since the Bragg condition is no longer satisfied over the entire crystal. However, the total efficiency of this method is much greater than that of the scanning method since the position sensitive detector can accumulate the entire spectrum at once. This method also has the advantage that source fluctuations do not present a problem as in the case of the scanning method.

Figure 3. Path of x rays (shaded area) emitted from an extended
source lcoated inside of the Rowland circle for the two
energies shown in Figure 2.

CURVED CRYSTAL

EXTENDED
SOURCE

POSITION
SENSITIVE
DETECTOR

ROWLAND CIRCLE
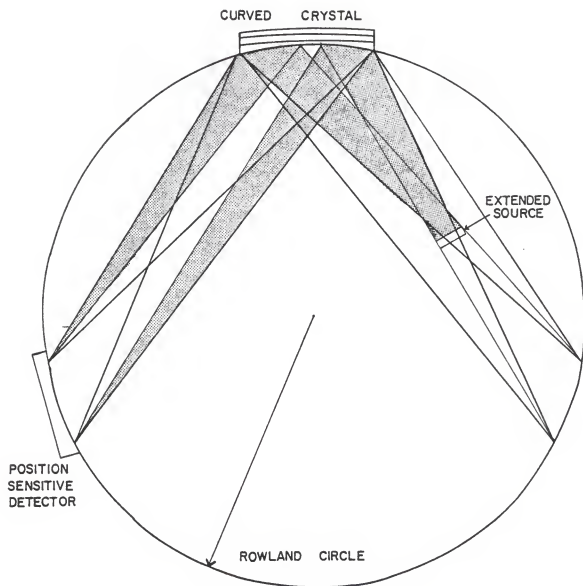
EXPERIMENTAL TECHNIQUES

An efficient Bragg crystal spectrometer has been designed to allow
for precision measurements of the Lyman-α x-ray energies of hydrogen-
like chlorine. The spectrometer has been tested by observing the Kα
x-ray spectra of argon in first order reflection from the crystal and
the Kα x-ray spectra of manganese in second order reflection. The Kα
x rays were produced by 3 MeV proton excitation of argon and manganese
targets using the EN tandem Van de Graaff accelerator at the James R.
MacDonald Laboratory at Kansas State University. Manganese spectra
were also acquired for electron and heavy-ion excitation to further
study the performance of the spectrometer. The argon and manganese
K$\alpha_{1,2}$ lines, which have accurately known energies and lie in close
proximity to the Cl Lyman-α lines, determine the energy calibration of
the spectrometer.

A. Spectrometer Design

The spectrometer, designed and built at Kansas State University,
utilizes a 2 inch x 1 inch curved quartz crystal obtained from the
National Bureau of Standards. The crystal has a Rowland circle of
one-meter radius in Johann geometry for the 110 crystal planes (d =
2.458 Å). X rays from the target are reflected from the crystal and
focused at a position sensitive "backgammon" x-ray detector, also
designed and built here at Kansas State University. A schematic of
the spectrometer is shown in Figure 4. The detector is located on the
Rowland circle 62 inches from the crystal at the focal point of the Ar
Kα_1 x rays. The argon and manganese targets were held in the target

Figure 4. Schematic of the Bragg crystal spectrometer with the manganese target and the argon gas cell (inset).

POSITION SENSITIVE DETECTOR

62"

63°

CURVED CRYSTAL SiO₂ (110)

31"

Mn TARGET

Ar GAS CELL

ION BEAM

ION BEAM

15
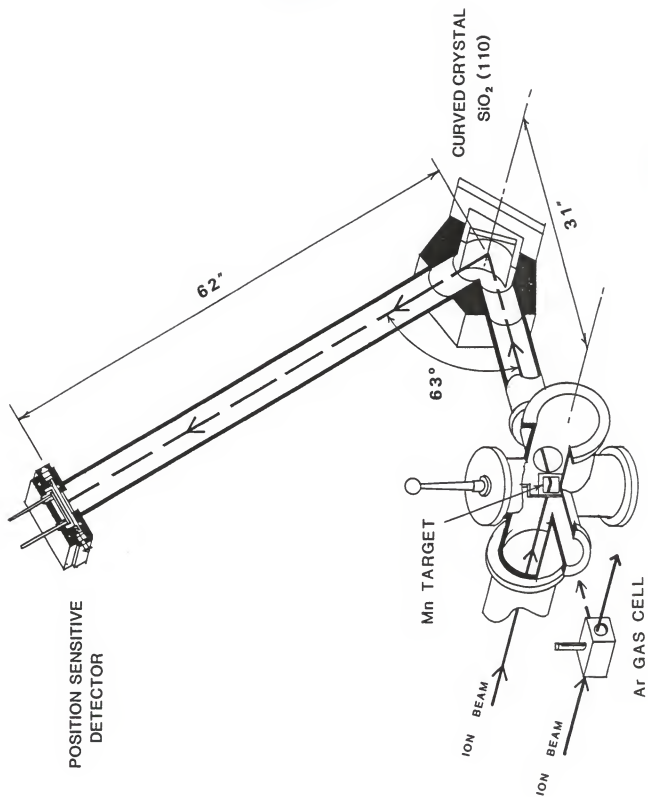
chamber at a point inside the Rowland circle 31 inches from the crystal. This placement was made considering the size of the target and allowing for x rays satisfying the Bragg condition within a small range of angles about the Ar $K\alpha_1$ Bragg angle to be reflected from the crystal and focused at the detector. The crystal is housed in a stainless steel chamber designed to allow the crystal to accept x rays within this predetermined range of angles. The crystal chamber is connected to the target chamber and to the detector by two-inch diameter aluminum beam pipe. Figure 5 shows the spectrometer at the experiment station on the accelerator beam line.

The crystal is mounted on an adjustable support held by the removable back plate of the crystal chamber as shown in Figure 6. The support allows for adjustments of the crystal orientation from outside the chamber while maintaining vacuum. Adjustments can be made for rotations of the crystal about two axes and for translation of the crystal normal to the plane of the back plate. This controls the position of the focal point of the x rays at the detector. Initial alignment of the crystal was made using a He-Ne laser. The laser was directed from the position of the target to the crystal, which was adjusted to reflect the beam to the position of the center of the detector.

The backgammon detector has a stainless steel chamber with outer dimensions of 3 x 5 x 1 5/8 inches. A cross-section of the detector is shown in Figure 7. The detector holds a chromium-plated glass board, also acquired from the National Bureau of Standards, that has a 70 μm intercathode gap insulating the two sides of the board in a backgammon design. The backgammon board and a 5 mil berylium x-ray

16

Figure 5. Spectrometer at the experiment station on the accelerator
beam line. The white 12-inch ruler lying on the horizontal
arm of the spectrometer indicates the scale of the picture.
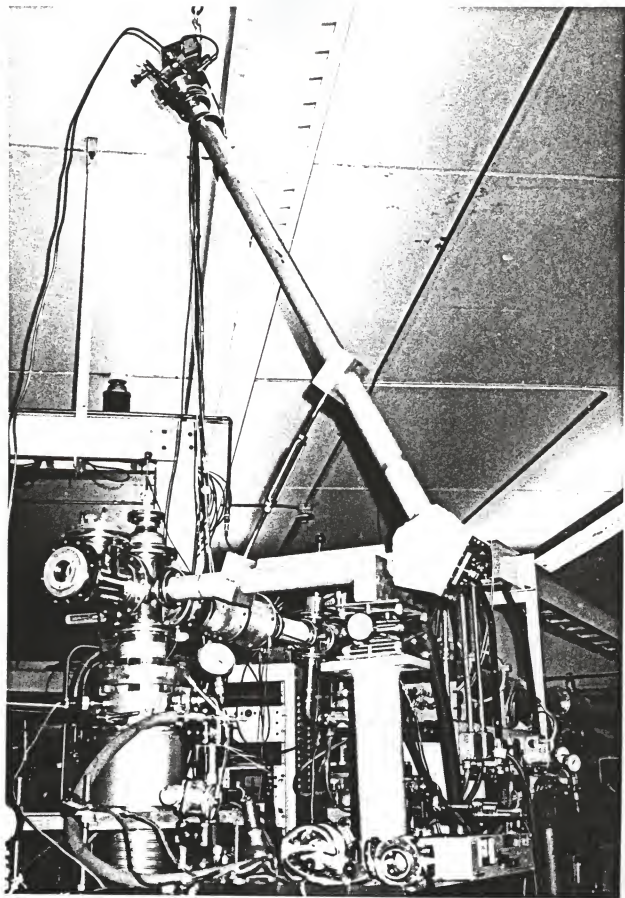
Figure 6. Adjustable crystal support held by the back plate of the
crystal chamber. The crystal can be rotated in two
directions (Bragg angle and tilt adjustments) and
translated in the direction normal to the plane of the
back plate (Rowland circle adjustment).

Top view

ADJUSTMENTS

Tilt

Rowland circle

Side view

Bragg angle

Tilt
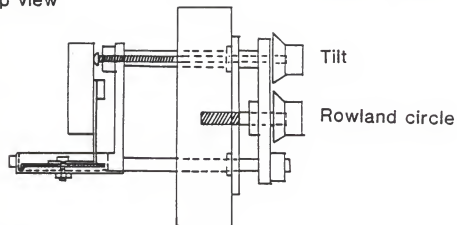
Figure 7. Cross-section of the backgammon detector. Shaded areas
represent insulators.

ANODE WIRE

X-RAY WINDOW

BACKGAMMON BOARD

HIGH VOLTAGE CONNECTOR

BACKGAMMON BOARD OUTPUTS

22

window form the front and back cathode planes in the detector. A 50 μm diameter tungsten anode wire is held midway between the back-gammon board and the berylium window which are separated by 0.5 in. The detector was filled 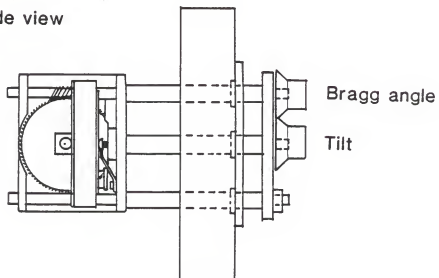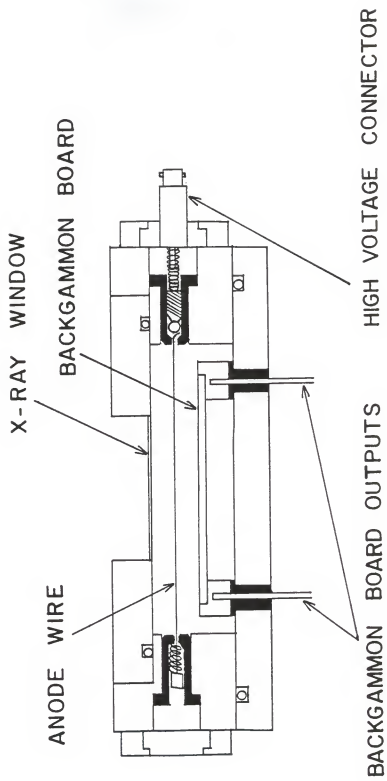with a 90% xenon – 10% methane mixture at pressures up to one atmosphere. The resolution of the detector was found to be independent of the detector gas pressure between one-half and one atmosphere and the pressure was held at approximately two-thirds atmosphere during data acquisition. Viton 0-rings and gaskets were used for the detector chamber and the gas outlets and electrical connectors to avoid contamination of the detector gas.

X rays enter the detector through the berylium window and are absorbed by the detector gas. Primary electrons produced in the ionization of the gas are accelerated toward the high-voltage anode wire, typically held at 1860 volts. Secondary electrons are produced in the collisions of the primary electrons with the atoms of the detector gas, creating a charge avalanche to the anode wire (the process occuring in normal gas proportional counters). The charge at the anode wire induces a charge on the backgammon board that is collected from each side of the board. The induced charge distribu-tion on the board can be modeled[19,20] using a point charge at the anode wire between two infinite parallel cathode planes. Using the method of images, the charge distribution $\sigma(x,y)$ induced on the cathode plane (forming the xy-plane) is found to be given by the expression:

$$\sigma(x,y) = -\frac{Q}{2\pi} \sum_{n=0}^{\infty} (-1)^n \frac{(2n+1) L}{[(2n+1)^2 L^2 + x^2 + y^2]^{3/2}}$$

where Q is the charge at the anode wire and L is the distance from the anode wire to the cathode. The origin (0,0) is taken as the projec-

23

tion of the point charge onto the cathode plane. The magnitude of the charge on each side of the backgammon board can be calculated by numerical integration of the charge density over each side of the board. The magnitude of the charge on a given side is found to be proportional to the position of the charge at the anode wire. This allows for the position of the charge at the anode wire, and thus the linear position of the detected x ray, to be found by measuring the magnitude of the charge from one side of the backgammon board normalized by the total charge from both sides. Since the x rays are energetically dispersed by the crystal, this measurement of the position then directly yields the energy of the x rays.

B. Data Acquisition

To obtain the argon spectra, Ar Kα x rays were produced by 3 MeV proton excitation using the EN tandem Van De Graaff accelerator schematically shown in Figure 8. Argon was contained in a closed gas cell at a pressure of approximately three quarters of an atmosphere. The gas cell had thin nickel entrance and exit windows for the proton beam and a 6μm aluminized mylar x-ray window viewed by the spectrometer at 90 degrees to the beam axis (cf. Figure 3). The proton beam could be defocused so that the effective size of the x-ray source, limited by the size of the nickel entrance window, was 1.2 x 2.2 cm^2. The Ar x rays were reflected from the crystal and focused at the detector.

The supporting electronics for signal analysis are diagrammed in Figure 9. The signals from each side of the backgammon board were amplified with equal gain by preamplifiers and Canberra 2020 spectroscopy amplifiers. The preamplifiers, acquired from Brookhaven

24

Figure 8. Schematic of the EN tandem Van de Graff accelerator at the
James R. MacDonald Laboratory at Kansas State University.

TANDEM VAN DE GRAAFF ACCELERATOR

EXPERIMENT STATIONS

SECONDARY ANALYZING MAGNET (SELECTS M, v, q)

POST STRIPPING FOIL (q~q')

OBJECT SLITS

PRIMARY ANALYZING MAGNET (SELECTS M, v, q)

TERMINAL VOLTAGE REGULATOR

IMAGE SLITS

ACCELERATOR

INFLECTION MAGNET (SELECTS M)

ION SOURCE
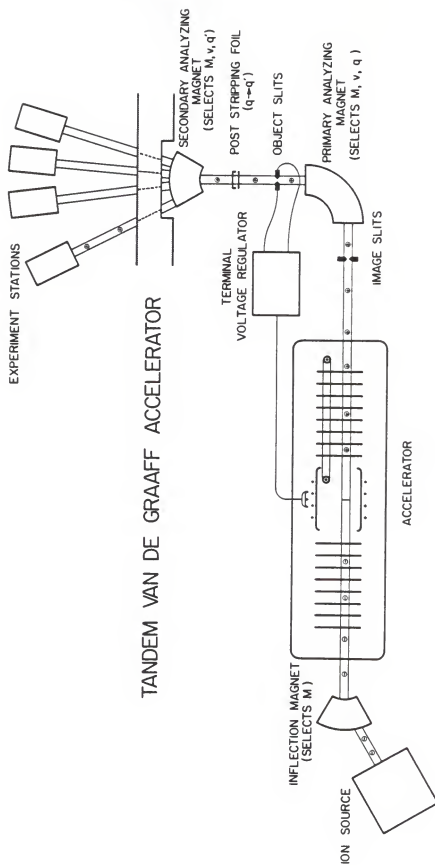
Figure 9. Block diagram of the electronics for backgammon detector signal analysis.

BACKGAMMON
BOARD

SIGNAL A   SIGNAL B

PREAMP   PREAMP

SPEC.   SPEC.
AMP   AMP

SUM AND   SUM AND
INVERT   INVERT

A   A + B

POSITION
SENSITIVE
DETECTOR
ANALYZER

$\frac{A}{A+B}$

A D C

MULTI -
CHANNEL
ANALYZER
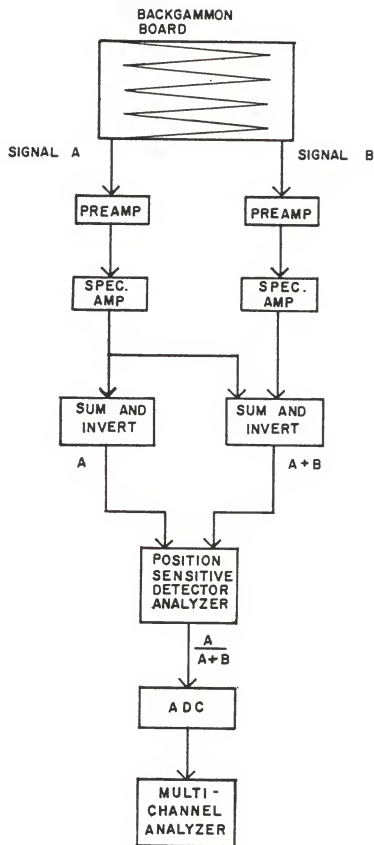
National Laboratory, were in the form of integrated circuit chips that were mounted directly to the back of the detector. The two amplified signals were added using a Tennelec TC253 dual sum and invert module, while one signal was sent through a separate dual sum and invert to maintain proper timing. The analog division of the signal from one side of the board by the sum of signals from both sides was performed by an Ortec 464 position sensitive detector analyzer. The resultant signal from this division was sent to an ADC and recorded by a multi-channel analyzer.

An energy spectrum for Ar $K\alpha$ x rays is shown in Figure 10 for all of the 1024 channels that were acquired. The spectrum shows the $K\alpha_1$ and $K\alpha_2$ diagram lines and the less intense satellite lines for a single L-shell vacancy prior to the radiative transition. A proton beam intensity of 400 nA gave a signal acquisition rate of approximately 150 counts per second and a total acquisition time of approximately one hour.

To acquire the manganese spectra, the gas cell was replaced by a solid manganese target, 2mm x 1.5cm x 1.5cm, set at 45 degrees to the incident beam. The electronics scheme for signal analysis was the same as that used for the argon data. A typical spectrum of the Mn $K\alpha$ x rays is shown in Figure 11. In the typical case of 1 μA of proton beam current on the target, the counting rate was approximately 400 counts per second and the spectrum acquisition time was about one-half hour.

Beams of 24 MeV C^{4+}, 23 MeV N^{4+}, 32 MeV O^{5+}, and 30 MeV F^{5+} were also run on the maganese target. The acquired spectra are shown in Figures 12 through 15, respectively. Most of the intensity in the

heavy-ion induced spectra is shifted to the satellite lines due to the high probability of multiple ionization by the highly charged projectiles.

A commerical electron gun was subsequently introduced into the beam line to produce 10 keV electrons. Figure 16 shows the Mn Kα x-ray spectrum for 10 keV electron excitation. This method of excitation allowed for lower satellite intensities but produced higher background counts due to bremsstrahlung radiation.
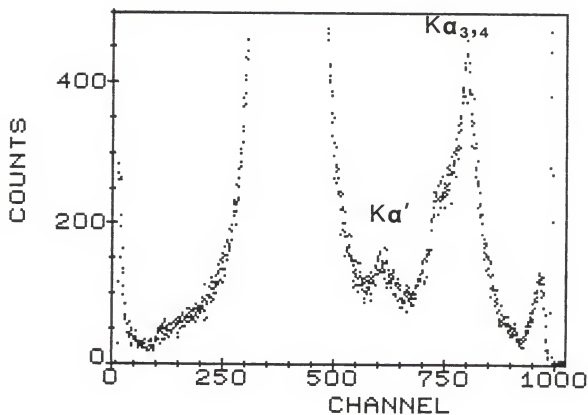
Figure 10. Ar Kα x-ray spectrum for 3 MeV H$^+$ → Ar.
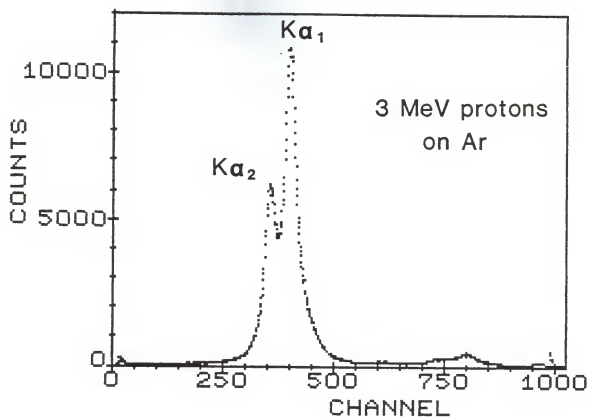
Figure 11. Mn Kα x-ray spectrum for 3 MeV H$^+$ → Mn.
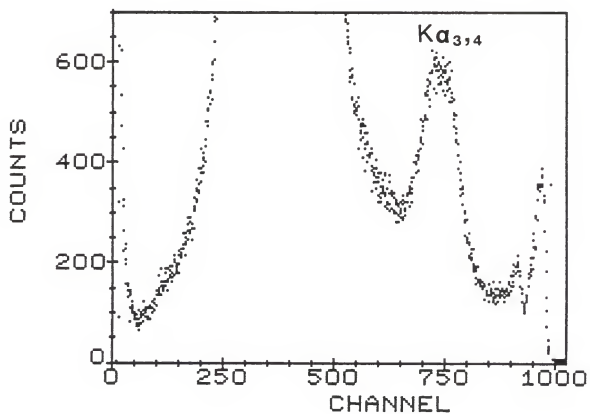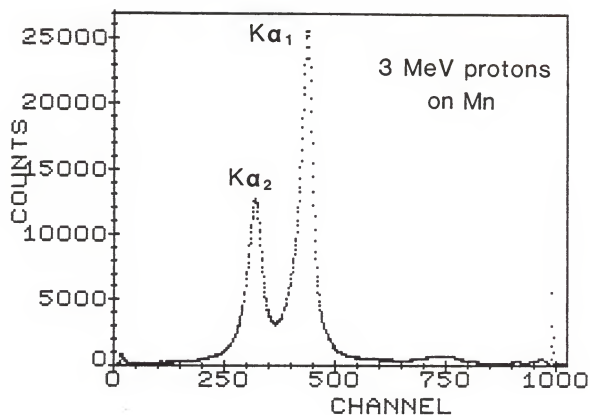
Figure 12. Mn Kα x-ray spectrum for 24 MeV C^{4+} → MN.

24 MeV C⁴⁺ on Mn spectrum showing COUNTS versus CHANNEL, with peaks labeled $K\alpha_2$, $K\alpha_1$, and $K\alpha_{3,4}$.
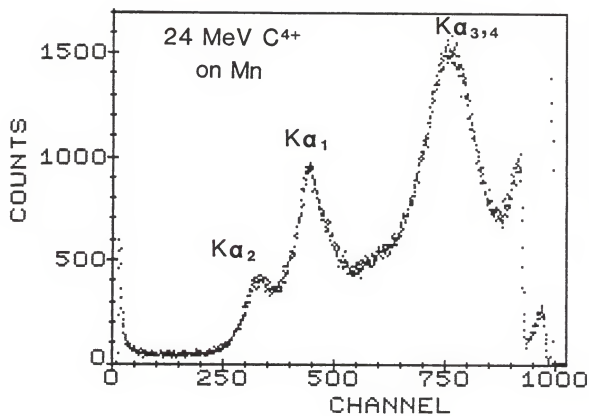
Figure 13. Mn Kα x-ray spectrum for 23 MeV N^{4+} → Mn.

23 MeV N⁴⁺ on Mn spectrum showing $K\alpha_2$, $K\alpha_1$, and $K\alpha_{3,4}$ peaks versus channel.

38
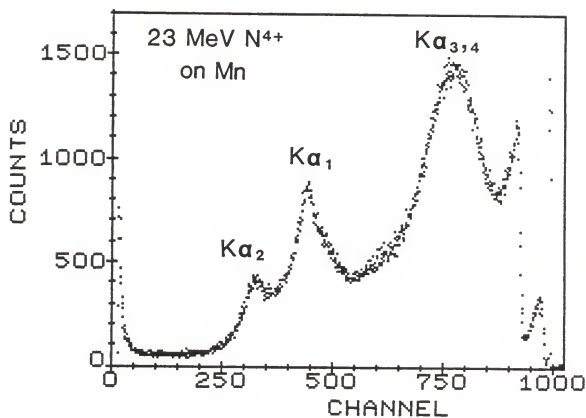
Figure 14. Mn Kα x-ray spectrum for 32 MeV O^{5+} → Mn.

32 MeV O⁵⁺ on Mn spectrum showing Counts vs. Channel, with peaks labeled $K\alpha_2$, $K\alpha_1$, and $K\alpha_{3,4}$.
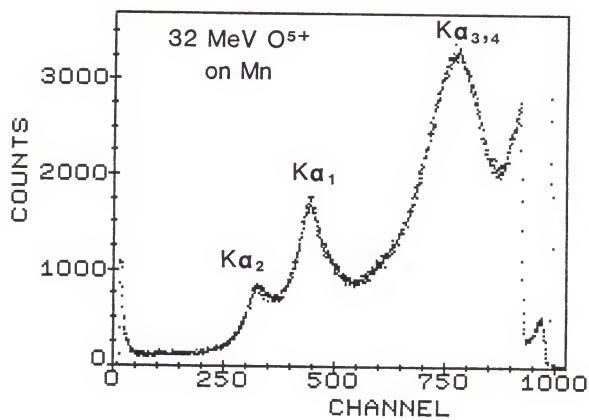
Figure 15. Mn Kα x-ray spectrum for 30 MeV $F^{5+} \rightarrow$ Mn.
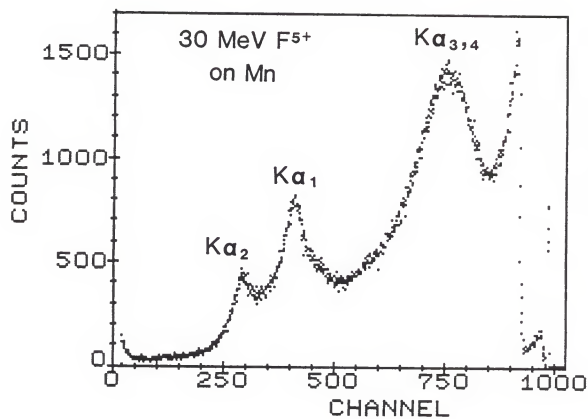
30 MeV F⁵⁺ on Mn spectrum showing $K\alpha_2$, $K\alpha_1$, and $K\alpha_{3,4}$ peaks of counts versus channel.

Figure 16. Mn Kα x-ray spectrum for 10 keV electron excitation.

Figure shows a spectrum: COUNTS (y-axis, with marks at 5000 and 10000) vs CHANNEL (x-axis, marks at 0, 250, 500, 750, 1000). Peaks labeled Ka₁ and Ka₂. Text in plot: "10 keV electrons on Mn".
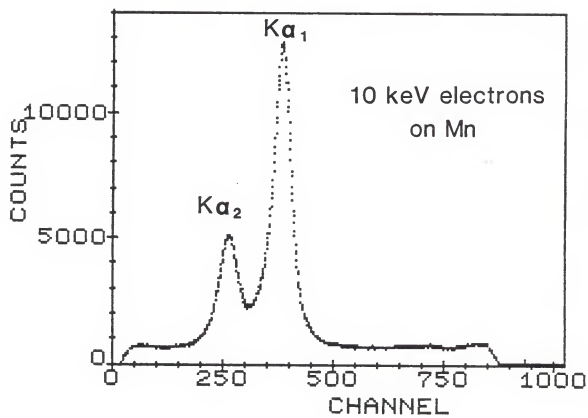
The energies of the $K\alpha_{1,2}$ diagram lines of argon and manganese
have previously been measured in high precision, allowing for these
lines to be used to study the linearity of the spectrometer. The Ar
$K\alpha_1$ and $K\alpha_2$ energies were recently measured[16] at the National Bureau
of Standards and found to be 2957.813 $\pm$ 0.008 and 2955.684 $\pm$ 0.013 eV,
respectively. The wavelengths of the Mn $K\alpha_1$ and $K\alpha_2$ lines were taken
from the tables published by Bearden[22] as 2.101820(9) and 2.10578(2)
Å*, respectively, where the errors for the rightmost digits are given
in paranthesis. These latter values were given relative to a Cu $K\alpha_1$
wavelength standard of 1.540562(2) Å*. The Mn $K\alpha$ wavelengths were
corrected for a recent determination of the Cu $K\alpha_1$ wavelength of
1.5405974 Å measured to 1 part per million by Kessler et al.[23]
Assuming a Gaussian error distribution, the errors given by Bearden,
quoted as probable errors (50% confidence intervals), were expanded to
one standard deviation (68% confidence interval). The corrected wave-
lengths were converted using $V\lambda = 12398.52$ eV·Å, which contributed no
appreciable error, giving Mn $K\alpha_1$ and $K\alpha_2$ energies of 5898.81 $\pm$ 0.04
and 5887.72 $\pm$ 0.09 eV, respectively.

The positions of the diagram lines in the 3 MeV proton induced
spectra were determined using a least-squares fitting program. The
spectral lines were modeled as approximate Voight functions[24] given by
the linear combination of a Lorentzian (L) and a Gaussian (G) function
of the form:

$$f(x;x_o,\Gamma,\eta) = \eta \; L(x;x_o,\Gamma) + (1-\eta) \; G(x;x_o,\Gamma)$$

$$= \eta \; [1+(\frac{x-x_o}{0.5\Gamma})^2]^{-1} + (1-\eta) \; \exp[-(\frac{x-x_o}{b\Gamma})^2]$$

where the linewidth Γ (full width at half maximum), shape parameter η, and mean x_o are fitted parameters and b is a constant equal to $(4 \ln2)^{-1/2}$. The fitting program allows for variable widths for each line but assigns the same lineshape.

The $K\alpha_{1,2}$ profile of argon was fit with a three-line model corresponding to the $K\alpha_{1,2}$ diagram lines and the $K\alpha''$ satellite line as shown in Figure 17. The fitted region is slightly larger than shown in the figure and the fit gave a value of χ^2 per degree of freedom of 1.6. The fitted lineshape is predominately Lorentzian ($\eta = 0.74 \pm 0.02$) suggesting that the resolution may be limited primarily by the natural linewidths of the spectral lines, although this is not strongly supported by comparing the fitted widths of the diagram lines, found to be 1.4 eV, to the semi-empirical value of 0.89 eV.[25] The statistical uncertainties (adjusted for χ^2) of the fitted means of the $K\alpha_1$ and $K\alpha_2$ lines are 0.101 and 0.082 channels, respectively, corresponding to 0.005 and 0.004 eV.

The Mn $K\alpha_{1,2}$ profile was fit with a four-line model corresponding to the two diagram lines and two satellite lines as shown in Figure 18. The two satellite lines were inferred from the high degree of asymmetry in the profile and are considered to represent groups of unresolved satellites. This approximation of the satellite contribution to the profile augments the rather large value of χ^2 per degree freedom of 2.9. The lineshape is given by $\eta = 0.67 \pm 0.02$ and the

46

Figure 17. Fitted lines to the Ar Kα x-ray spectra for 3 MeV proton
excitation.

3 MeV protons on Ar
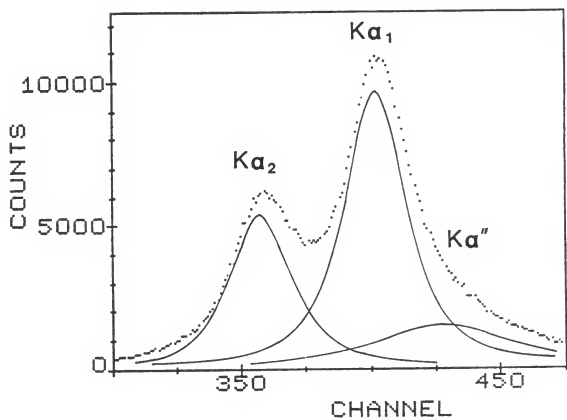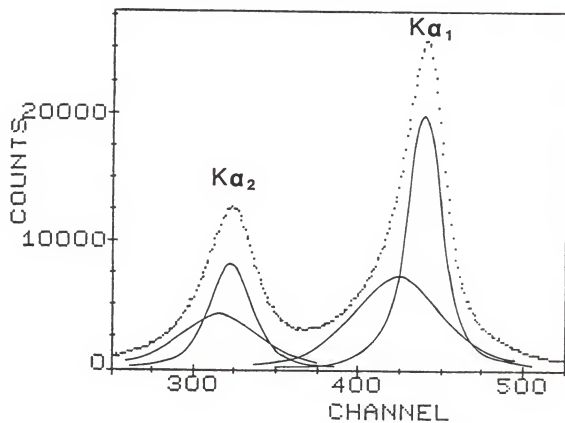
Figure 18. Fitted lines to the Mn Kα x-ray spectra for 3 MeV proton
excitation.

3 MeV protons on Mn

fitted widths of the $K\alpha_1$ and $K\alpha_2$ lines are 2.4 and 2.9 eV, respectively, as compared to the semi-empirical values of 1.48 and 1.50 eV.[25] The statistical uncertainties of the means of the $K\alpha_1$ and $K\alpha_2$ lines are 0.065 and 0.173 channels, respectively, corresponding to 0.006 and 0.017 eV.

The large values of χ^2 per degree of freedom of the fits are attributed primarily to contributions to the line profiles from unresolved satellites. In the fits to all of the spectra, the number of lines in the model were varied until a reasonable fit was obtained and considered to best represent the physical nature of the spectrum.

To observe the linearity of the spectrometer, spectra were acquired for argon and manganese in two consecutive runs in which all parameters of the experiment were held constant (such as the crystal orientation). The fitted positions (in channels) along with the known energies of the $K\alpha_{1,2}$ diagram lines serve as calibration values which are plotted in Figure 19 (the Mn $K\alpha_{1,2}$ energies have been divided by 2 corresponding to second-order diffraction). A line of the form $E = \alpha + \beta \cdot (\text{channel})$ was least-squares fit to these values, weighted by the uncertainties in both the energies and positions (the uncertainity in the position was converted to an energy value using 0.0483 eV/channel. This was added in quadrature to the uncertainty in the known energy, giving a total uncertainity in the energy used to weight the fit). The fit gave a value for χ^2 of 6.1 for the line defined by $\alpha = 28.088 \pm 0.048$ eV and $\beta = 0.0482 \pm 0.001$ eV/channel. The difference of the energy values of the calibration points and the corresponding energy values of the fit line are plotted in Figure 20.

Attempts to fit the $K\alpha_{1,2}$ lines in the heavy-ion induced Mn

51

Figure 19.   Initial calibration of the spectrometer using the argon
and manganese $K\alpha_{1,2}$ diagram lines.   The errors of the
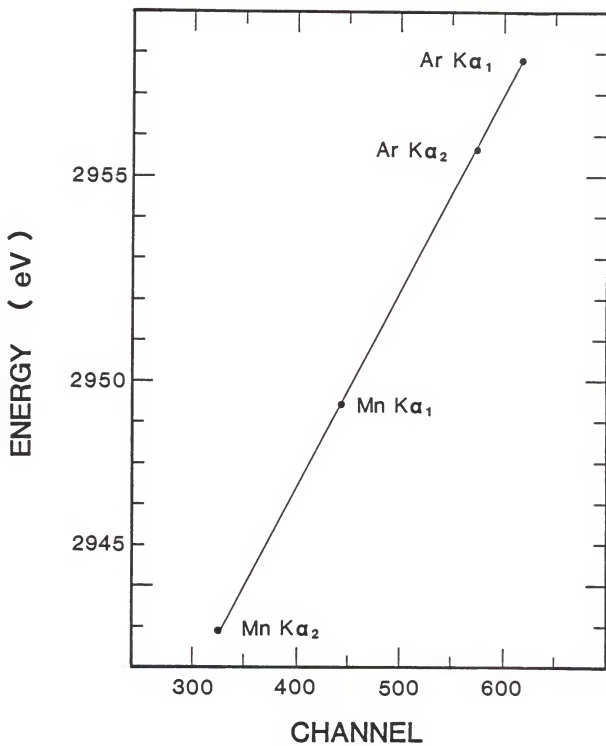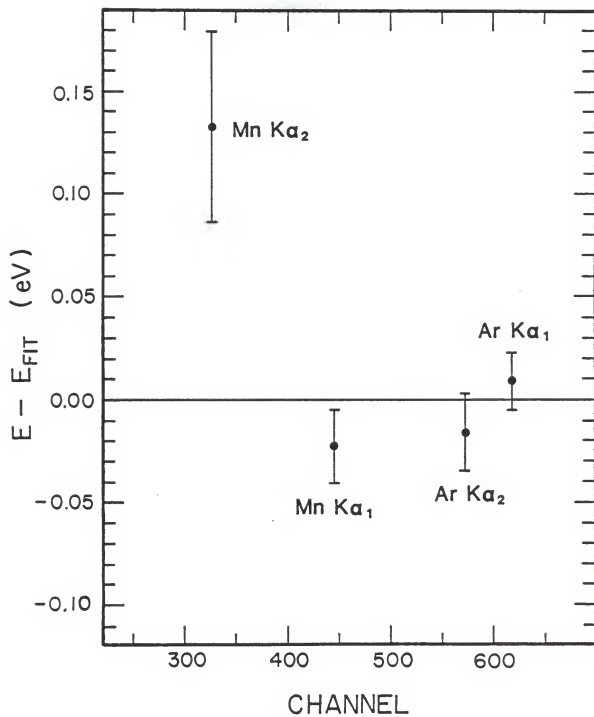values are within the size of the data points.

Figure 20. Difference of the energy values of the calibration points
and the corresponding values of the fit line, showing the
nonlinearity of the calibration points.

spectra proved unsuccessful due to the strong dependence of the fit on the model used for the satellite lines. This dependence is expected since the low-energy wing of the $K\alpha_{3,4}$ peak (and higher satellites) contributes significantly to the intensity in the region of the $K\alpha_{1,2}$ lines. The resolution was insufficient to identify single lines in the $K\alpha_{3,4}$ peak such that varying the number of lines in the model proved the fits to this region to be nonphysical. This inability to fit the satellite lines disallowed an acceptable fit of the $K\alpha_{1,2}$ lines.

In the Mn spectra produced by 10 keV electron excitation, the $K\alpha_{1,2}$ profile was fit with four lines and a constant background (associated with the counts due to bremstralung radiation). No significant differences were found in the fitted diagram lines compared to those in the proton induced spectra.

Discussion of Results

The 1s Lamb shift in hydrogenlike chlorine (S(1s) = 0.938 eV) is 317 parts per million of the calculated Lyman-α_1 transition energy (E(Lyα_1) = 2962.376 eV).[7] To experimentally determine the 1s Lamb shift to an accuracy of 10% then requires the accuracy of the measurement of the Lyman-α energies to be on the order of 30 parts per million, while it is further proposed that a determination of the 1s Lamb shift can be achieved to within 1%.[15] To reach this degree of accuracy, the transfer calibration must be extremely precise. In terms of this high level of precision, the calibration values presented in the previous chapter deviate considerably from linearity, as is evident from Figure 19.

One factor in the calibration that must be considered is the assignment of the energies determined in previous measurements to the models used to fit the calibration spectra. In this respect, the determination of an actual x-ray energy corresponding to a certain transition is not what is important, nor what is sought. For the purposes of the calibration, what is required is the determination of a "bench mark" to which to assign a known energy. A reasonable amount of confidence can be felt in assigning the argon energies obtained from the National Bureau of Standards to the fitted K$\alpha_{1,2}$ lines, since they used the same model (approximate Voight functions, 3 lines) in their energy determination. Even with the same model however, small discrepancies may exist due to different sizes of the fit region, unequal resolution, and different satellite intensities from different

57

modes of excitation. The primary concern in this factor of the calibration is the assignment of the energies determined from the Bearden tables to the fitted Mn $K\alpha_{1,2}$ lines. According to the tables, a wavelength value was assigned to the point of maximum intensity in the line profile determined by the method of division of chords.[25] This is a graphical method that was used before computer fitting techniques were available that involves locating the midpoints of chords drawn across the line profile at several intervals (50% of the maximum, 60%, 70%, etc.) and then extrapolating a smooth curve drawn through the midpoints to the "peak" position, or point of maximum intensity. An analysis of different models used to fit spectral lines has recently been made by M. P. Stockli[26,27] here at Kansas State University. The points of maximum intensity of Mn $K\alpha_{1,2}$ lines were determined with least-squares fits of different degrees of polynomials to the line profiles (taken above 50% of the maximum) and to the differentials of the line profiles (given by $N(x) - N(x - 1)$, where $N(x)$ is the number of counts in channel x). These results were compared with the results obtained from fits of different line models (i.e., models assuming certain distributions). It was found that the fitted position of maximum intensity may differ from the fitted mean of a distribution line by 0.27 eV due to the asymmetry in the line profile from satellite contributions. This indicates that a correction may be needed in relating the manganese energies determined from the Bearden tables to the fitted diagram lines, although the relationship between Bearden's fits and the polynomial fits has not yet been determined. It was also found that the polynomial fits gave larger statistical uncertainties in the peak positions than the fits using

distribution models, so that the polynomial fits may not be as well suited for high-precision measurements.

The nonlinearity of the argon and manganese calibration points can be attributed mainly to the intrinsic nonlinearity of the backgammon detector. The properties of a similar detector have been studied by Duvall et al.[20] at the National Bureau of Standards. The linearity of their detector was determined using a collimated x-ray beam and a set of slits accurately positioned in front of the detector. Using a signal analysis procedure similar to that described previously (Chapter 2), the spectrum generated from the slit image was fit with a Gaussian distribution and a plot was made of the peak position as a function of the slit position. The derivative of this linearity curve was also given which, by scaling to the detector used here, allowed for an estimate to be made of the correction to the channel numbers of the argon and manganese calibration lines. The magnitude of the correction increases with the distance from the center of the back-gammon board so that the largest correction, $- 4.5 \pm 0.5$ channels, was made to the Mn $K\alpha_2$ line. When the corrected calibration points were again fit with a line, it was found that the degree of nonlinearity of the calibration points had increased as indicated by a worse fit ($\chi^2 = 15.3$). This implies that a more accurate knowledge of the linearity of the detector is required, such as can be obtained through a mapping procedure as described above.

The main correction to the calibration points will be for the non-linearity of the detector. Along with this correction and the possible correction to the manganese energies for different fitting techniques, a final correction in the calibration of the spectrometer

will be made to the manganese energies for diffraction in second order
(the argon and chlorine x rays are reflected in first order). Further
analysis of these corrections was in progress at the time of this
writing.

Chapter V

PROPOSED 1s LAMB SHIFT MEASUREMENT

The previous measurement of the 1s Lamb shift in hydrogenlike chlorine performed by Richard et al.[16], of which the work presented in this thesis is an extention, used the method of beam-foil excitation to observe the Lyman-α x rays. The primary limiting factor in this method is attributed to the large doppler shift in the x-ray energies due to the high velocity of the ions. This effect can be minimized by accurate alignment of the spectrometer to 90-degree geometry using optical techniques, although a contribution to the x-ray energies from the transverse doppler shift will inevitably be seen. This effect was studied by Richard et al.[16] by varying the projectile velocity, and the resulting Lyman-α x-ray spectra are shown in Figure 21. The energy calibration of the spectra was made using the Ar $K\alpha_1$, $K\alpha_2$, and $K\alpha_4$ lines. Figure 22 shows the shifted chlorine Lyman-$\alpha_{1,2}$ energies in relation to the argon and manganese calibration lines that have been presented in this thesis. This shows the suitability of the position of these lines to be used for the transfer calibration in the chlorine Lyman-α measurement.

Along with the analysis of the corrections discussed in the previous chapter, the next step in the development of the spectrometer will involve attempting to increase the resolution with alternate techniques for signal analysis. One such technique would replace the analog division of the charge collected from the backgammon board by the division of the digitizied signals by a computer. The resolution of this spectrometer is inherently increased from that obtained in the previous chlorine 1s Lamb shift measurement due to the increased

Figure 21. Chlorine Lyman-α x-ray spectra for various chlorine
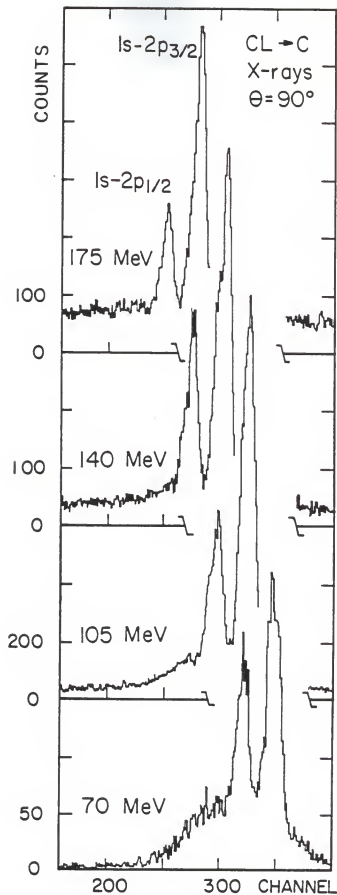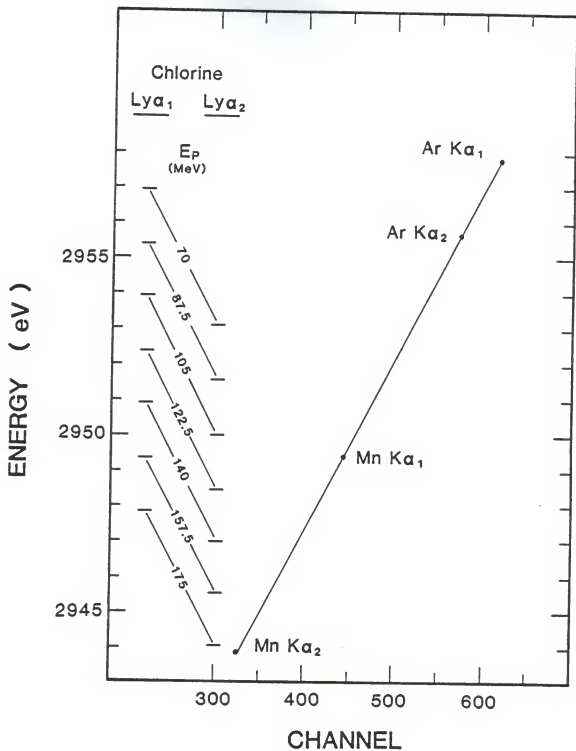projectile energies from Richard et al.[16]

Figure 22. Doppler shifted chlorine Lyman–α energies for various
projectile energies E_p from Richard et al.[16] in relation
to the argon and manganese calibration lines.

wavelength dispersion from operating at a larger Bragg angle. Increasing the resolution decreases the uncertainties in the fits to the spectra, allowing for an increase in the precision of the Lyman-α measurements and thus increasing the accuracy of the determination of the 1s Lamb shift.

A preliminary measurement of the chlorine Lyman-α x rays will be made to further test the spectrometer. One of the limiting factors in the precision Lyman-α measurements is due to the unknown satellite contributions to the lineshape of the Lyman-$\alpha_{1,2}$ lines which introduce difficulties in modeling the spectra to accurately determine the x-ray energies. The increased resolution of this spectrometer should allow for a better understanding of this satellite structure. This measurement will also test the response of the spectrometer to the low intensities of the Lyman-α x rays. This preliminary measurement will be performed at either Argonne National Laboratory or Brookhaven National Laboratory.

REFERENCES

1. W.V. Houston, Phys. Rev. $\underline{51}$, 446 (1937).

2. R.C. Williams, Phys. Rev. $\underline{54}$, 558 (1938).

3. S. Pasternack, Phys. Rev. $\underline{54}$, 1113 (1938) interpreted the results of Houston[1] and Williams[2] as due to a shift in the 2s level.

4. W.E. Lamb, Jr. and R.C. Retherford, Phys. Rev. $\underline{72}$, 241 (1947).

5. Given in most atomic spectra texts, such as Bethe and Salpeter, in Quantum Mechanics of One- and Two- Electron Atoms (Plenum, New York, 1977), p. 68.

6. H.A. Bethe, Phys. Rev. $\underline{72}$, 339 (1947).

7. P.J. Mohr, At. Data and Nucl. Data Tables $\underline{29}$, 453 (1983).

8. S.R. Lundeen and F.M. Pipkin, Phys. Rev. Lett. $\underline{46}$, 232 (1981).

9. H. Gould and R. Marrus, Phys. Rev. Lett. $\underline{41}$, 1457 (1978).

10. O.R. Wood, II, C.K.N. Patel, D.E. Murnick, E.T. Nelson, M. Leventhal, H.W. Kugel, and Y. Niv, Phys. Rev. Lett. $\underline{48}$, 398 (1982).

11. H.W. Kugel and D.E. Murnick, Rep. Prog. Phys. $\underline{40}$, 297 (1977).

12. T.W. Hansch, S.A. Lee, R. Wallenstein, and C. Wieman, Phys. Rev. Lett. $\underline{34}$, 307 (1975).

13. J.P. Briand, M. Tavernier, P. Indelicato, R. Marrus, and H. Gould, Phys. Rev. Lett. $\underline{50}$, 832 (1983).

14. M. Tavernier, J.P. Briand, P. Indelicato, D. Liesen, and P. Richard, J. Phys. B $\underline{18}$, L327 (1985).

15. As reported by P. Richard and M. Stockli, Proceedings of the 8th Conference on Application of Accelerators in Research and Industry (Denton 1984), Nucl. Instr. and Meth., to be published.

16. P. Richard, M. Stockli, R.D. Deslattes, P. Cowan, R.E. LaVilla, B. Johnson, K. Jones, M. Meron, R. Mann, K. Schartner, Phys. Rev. A $\underline{29}$, 2939 (1984).

17. H.F. Beyer, R.D. Deslattes, F. Folkmann, and R.E. LaVilla, J. Phys. B, to be published.

18. E. Kallne, J. Kallne, P. Richard, and M. Stockli, J. Phys. B $\underline{17}$, L115 (1984).

19. R.D. Deslattes, R. Schuch et al., private communications.

20. B.P. Duvall, J. Barth, R.D. Deslattes, A. Henins, and G.G. Luther, Nucl. Instr. and Meth. $\underline{222}$, 274 (1984).

21. I. Endo, T. Kawamoto, Y. Mizuno, T. Ohsugi, T. Taniguchi, and T. Takeshita, Nucl. Instr. and Meth. $\underline{188}$, 51 (1981).

22. J.A. Bearden, Rev. Mod. Phys. $\underline{38}$, 78 (1967).

23. E.G. Kessler, Jr., R.D. Deslattes, and A. Henins, Phys. Rev. A $\underline{19}$, 215 (1979).

24. G.K. Wertheim, M.A. Butler, K.W. West, and D.N.E. Buchanan, Rev. Sci. Instrum. $\underline{45}$, 1369 (1974).

25. M.O. Krause and J.H. Oliver, J. Phys. Chem. Ref. Data $\underline{8}$, 329 (1979).

26. J.A. Bearden, Phys. Rev. $\underline{43}$, 94 (1933).

27. M.P. Stockli, private communications.

28. M.P. Stockli, J.L. Shinpaugh, J.M. Sanders, and P. Richard, BAPS $\underline{30}$ (1985).

DESIGN OF A HIGH-EFFICIENCY HIGH-RESOLUTION

X-RAY SPECTROMETER

FOR

1s LAMB SHIFT MEASUREMENTS

by

JEFFERSON L. SHINPAUGH

B.S., Kansas State University

———————————

AN ABSTRACT OF A MASTER'S THESIS

submitted in partial fulfillment of the

requirements for the degree

MASTER OF SCIENCE

Department of Physics

KANSAS STATE UNIVERSITY

Manhattan, Kansas

1985

ABSTRACT

An efficient Bragg crystal spectrometer has been designed to allow
for precision measurements of the Lyman-α x-ray energies of hydrogen-
like chlorine. The spectrometer utilizes a curved quartz crystal with
a one-meter Rowland circle and a position sensitive "backgammon" x-ray
detector. The spectrometer has been tested by observing the argon Kα
x-ray spectra in first order reflection from the crystal and the
manganese Kα x-ray spectra in second order reflection. The Kα x rays
were produced by 3 MeV proton excitation. Manganese spectra were also
acquired for electron and heavy-ion excitation to further observe the
performance of the spectrometer and to study the possible dependance
of the fitted positions of the K$\alpha_{1,2}$ diagram lines on the mode of
excitation. The argon and manganese K$\alpha_{1,2}$ lines, which have
accurately known energies and lie in close proximity to the chlorine
Lyman-α lines, determine the energy calibration of the spectrometer.
The precision measurement of the chlorine Lyman-α energies will allow
for an experimental determination of the $1s_{1/2}$ Lamb shift.